2018

Investigation of novel inverted NiO@NixCo1-xO core-shell nanoparticles

Samiul Hasan
MSU Undergraduate

R. A. Mayanovic
Missouri State University

Mourad Benamara

Investigation of novel inverted NiO@$Ni_xCo_{1-x}O$ core-shell nanoparticles

Samiul Hasan,[1,a] R. A. Mayanovic,[1] and Mourad Benamara[2]
[1]*Department of Physics, Astronomy and Materials Science, Missouri State University, Springfield, MO 65897, USA*
[2]*Institute for Nano Science and Engineering, University of Arkansas, Fayetteville, AR 72701, USA*

(Presented 8 November 2017; received 26 September 2017; accepted 24 October 2017; published online 11 December 2017)

Inverse core-shell nanoparticles, comprised of an antiferromagnetic (AFM) core covered by a ferromagnetic (FM) or ferrimagnetic (FiM) shell, are of current interest due to their different potential application and due to the tunability of their magnetic properties. The antiferromagnetic nature of NiO and high Néel temperature (523 K) makes this material well suited for inverse core-shell nanoparticle applications. Our primary objective in this project has been to synthesize and characterize inverted core-shell nanoparticles (CSNs) comprised of a NiO (AFM) core and a shell consisting of a $Ni_xCo_{1-x}O$ (FiM) compound. The synthesis of the CSNs was made using a two-step process. The NiO nanoparticles were synthesized using a chemical reaction method. Subsequently, the NiO nanoparticles were used to grow the NiO@$Ni_xCo_{1-x}O$ CSNs using our hydrothermal nano-phase epitaxy method. XRD structural characterization shows that the NiO@$Ni_xCo_{1-x}O$ CSNs have the rock salt cubic crystal structure. SEM-EDS data indicates the presence of Co in the CSNs. Magnetic measurements show that the CSNs exhibit AFM/FiM characteristics with a small coercivity field of 30 Oe at 5 K. The field cooled vs zero field cooled hysteresis loop measurements show a magnetization axis shift which is attributed to the exchange bias effect between the AFM NiO core and an FiM $Ni_xCo_{1-x}O$ shell of the CSNs. Our ab initio based calculations of the $Ni_xCo_{1-x}O$ rock salt structure confirm a weak FiM character and a charge transfer insulator property of the compound. https://doi.org/10.1063/1.5006687

I. INTRODUCTION

Bimagnetic core-shell nanoparticles (CSNs) are of considerable interest due to their potential applications in magnetic spin valves, spintronics, magnetic random access memory, hyperthermia, MRI imaging, drug delivery and in other areas.[1–4] The magnetic properties of bimagnetic CSNs (without being embedded in a surrounding matrix) are tuned by adjustment of overall size, core vs shell size, core vs shell composition, and morphology. Core-shell nanoparticles are typically fabricated in a conventional configuration, having a ferromagnetic (FM) core and an antiferromagnetic (AFM) or ferrimagnetic (FiM) shell, or in an inverted configuration, having an AFM core and a FM or FiM shell. Due to their highly ordered AFM cores, the inverted bimagnetic CSNs have highly tunable coercivities, blocking temperatures, and other magnetic properties that are highly promising for device and medicinal applications. There has been particular attention paid to the exchange bias effect in bimagnetic CSNs, whereby a magnetic interaction between the core and shell has a direct bearing on the overall magnetic properties of the nanostructures.[5,6] By suitable tuning of the CSNs in terms of composition, size and morphology characteristics alluded to above, the exchange bias properties can potentially be exploited for various magnetic device and medicinal applications.

[a]Corresponding author: Samiul Hasan, email: samiul097@live.missouristate.edu, samiul.hasan.001@gmail.com

We have recently investigated a number of Cr_2O_3@$M_xCr_{2-x}O_{3-\delta}$ CSN systems and found these to have enhanced magnetic properties that show promise for potential magnetic applications.[7–9] However, the exchange bias effect in these CSNs has been observed to be considerably reduced at room temperature due to the Néel temperature of the AFM core occurring just above the RT value (T_N = 308 K). Bulk NiO generally has AFM ordering with a Néel temperature considerably above room temperature (T_N = 523 K), which makes it well suited for bimagnetic core-shell nanostructure applications. Remarkably, to our knowledge, with the exception of a very small number of other systems, the Ni@NiO CSNs appear to be the overwhelmingly predominant bimagnetic NiO-based core-shell nanostructure system that has been investigated to date.[10–15] The synthesis of Ni@NiO CSNs typically involves synthesis of the Ni nanoparticles followed by their oxidation, thus producing a NiO shell over the Ni core. These CSNs have been shown to exhibit high coercivities at room temperature[15] and, for ones coated with graphitic carbon, superparamagnetic blocking temperatures at above room temperature value.[13] In both cases, these effects were attributed to substantial exchange bias effects occurring at the interface between the FM Ni core and the AFM NiO shell. Recently, Skoropata et al. studied a series of iron oxide based core-shell nanostructures, including γ-Fe_2O_3@NiO CSNs.[16] Their conclusion was that the magnetic properties of the γ-Fe_2O_3@NiO CSNs were consistent with the formation of an inter-diffused Ni-doped Fe_2O_3 layer at the core-shell interface, resulting in a trilayer nanostructure. Although most likely not bimagnetic, it has been reported that SiO_2@NiO CSNs exhibit greater remanent and saturation magnetization values, but lower coercivities, than NiO nanoparticles.[17] Ponnusamy et al. have recently synthesized Co-doped NiO nanoparticles using a chemical reaction method.[18] The authors report that their magnetic measurements reveal ferromagnetic properties in the $Co_xNi_{1-x}O$ nanoparticles. In this paper, we report on the synthesis and characterization of inverted NiO@$Ni_xCo_{1-x}O$ CSNs, where the core-shell nanostructure was made using our hydrothermal nanophase epitaxy method.[7–9]

II. METHODS

The synthesis of the CSNs was made as follows: NiO nanoparticles were first synthesized according to procedures outlined by El-Kemary et. al.[19] The nanoparticle synthesis was made using thermal decomposition of $Ni(OH)_2$. A precursor was first prepared using nickel chloride hexahydrate (0.111 M) dissolved in ethanol which was then added to 6.73 ml of hydrazine monohydrate at a solution molar ratio of 5. KOH was used to adjust the pH to about 12 and the solution was stirred for ~2 hours at 22 °C. Upon completion of stirring, the reaction product was rinsed with deionized water for removal of residues and then centrifuged in tolune. The $Ni(OH)_2.0.5H_2O$ nanoparticles were dried in atmosphere. Finally, the nickel hydroxide nanoparticles were converted to NiO nanoparticles through thermal decomposition at 600 °C for ~2 hours.

The NiO nanoparticles were next used as cores to synthesize the NiO@$Ni_xCo_{1-x}O$ CSNs using a hydrothermal method described previously.[20] First, HPLC grade water (pH = 7) was purged with N_2 gas for 15 minutes at 70 °C. Next, 0.237 g $CoCl_2.6H_2O$ were added to the deoxygenated water to make a 0.05 M solution (pH = 5.6) and sonicated for ~30 minutes. Several drops of HCl were added to reduce the pH of the solution to a value of 3.2. Subsequently, 0.33g of NiO nanoparticles was added to the solution, which was then sonicated for ~30 minutes. Subsequently, the solution was inserted inside an autoclave and hydrothermal treated at ~190 °C for 20 hours. The resulting NiO@$Ni_xCo_{1-x}O$ CSNs were then rinsed, centrifuged in DI water and subsequently dried in atmosphere.

The SEM imaging characterization was made using a JEOL SEM instrument operating at 2 kV with WD of 5 mm. The samples were mounted on carbon tape for SEM imaging. Preliminary elemental analysis was made using a SEM-EDS (Oxford Instruments) and a field emission gun. XRD data were measured from the nanopowder samles using a Bruker D8 Discover diffractometer operating at 40 kV and 40 mA. The diffractometer is operated using a Cu tube x-ray source (Cu Kα, λ= 1.54184 Å), a Göbel mirror and a 0.6 mm slit on the incident x-ray beam. A Linxeye 1-D Si strip detector was used for measurement of the XRD data. The XRD data were analyzed using Rietveld refinement, which was accomplished using the Bruker TOPAS software. The modelling of the background in the XRD patterns was made using a 5-th order Chebychev polynomial.

The magnetization data were measured from the samples using a SQUID MPMS/XL magnetometer (Quantum Design) and a PPMS-VSM instrument at CCMR, Cornell University (Quantum Design). The nanoparticle samples were packed in a gelatin capsule and then inserted inside the dewar of the SQUID magnetometer. The magnetization data were measured in the 5 – 300 K temperature (T) range. An applied field of 500 Oe was used to make the magnetization vs T measurements in the field-cooled (FC) case. The magnetic hysteresis curves were measured at 5 K in the -10,000 to 10,000 Oe applied field range. The samples were cooled at 20,000 Oe in the case of FC hysteresis loop measurements whereas 0 field was applied in the case of zero-field-cooled (ZFC) measurements. The TEM analysis was made using a Titan 80-300 instrument for which the field emission gun was operated at 300 keV. The TEM samples were prepared on lacey carbon grids.

The first principles calculations were made using the local spin density approximation method (LSDA) implemented in Quantum Espresso.[21] A rhombohedral primitive unit cell of NiO with a space group of $Fm\bar{3}m$ (COD 4329325) was used for the self-consistent field calculations. The $Ni_{0.88}Co_{0.12}O$ structure was constructed by replacement of one of the Ni (out 8 cation sites) with Co in the 1 x 2 x 2 supercell. Calculation convergence was achieved with a net antiferromagnetic configuration (+-+-) for the NiO structure. The Brillouin zone integral 6 x 6 x 6 point grid was used based on the Monkhorst–Pack scheme.[22] The cutoff energy for the plane waves was 150 eV. Structural relaxation (volume) was accomplished for all of the structures and the relaxed structural parameters were used in the final calculation. Density of states (DOS) and the projected density of state (pDOS) were obtained by using the tetrahedron method with an 8 x 8 x 8 k-point grid mesh. Perdew–Burke–Ernzerhof exchange-correlational norm conserving pseudopotentials were used for all the atoms.[23] Additionally, in order to describe the electron-electron correlation characteristics of local electrons in transition metal atoms, we have performed the GGA+U type calculation where U is the on-site Coulomb energy, U and the exchange interaction (J) were used.

III. RESULTS AND DISCUSSION

Fig. 1(a) shows an SEM image of synthesized CSNs. A Gaussian fit of the histogram plot of particle size distribution shown in Fig. 1(b), as determined from TEM imaging, gives an average particle size of 29.7(2) nm for the NiO@$Ni_xCo_{1-x}O$ CSNs. This is in very good agreement with our XRD Scherrer equation analysis yielding a CSN size of 29.39(6) nm. The SEM-EDS data shown in Fig. 1(c) show that Co, along with Ni and O, are present in the sample. Fig. 1(d) shows a high-resolution TEM (HRTEM) image of an isolated CSN. As shown in the TEM image, the core and shell are separated by an interface which is slightly more structurally disordered than either the core or the shell of the isolated CSN. The SEM and TEM imaging indicate presence of faceted as well as pseudospherically shaped CSNs. The shell region of the nanoparticle shown in Fig. 1(d) is not completely uniform as the core NiO nanoparticles are pseudospherical in shape. The approximate thickness of the shell, estimated from the TEM images, is ~2 nm. The shell and core regions of the CSNs, respectively, have identical crystallographic symmetry, as evidenced from our TEM and XRD results (Figs. 1(d and e)), providing evidence of epitaxial growth of the shell. Fig. 1(e) shows the powder x-ray diffraction pattern measured from our CSNs at room temperature. XRD analysis indicates that the CSNs possess the FCC structure with space group $Fm\bar{3}m$ with a small contribution from a minor cubic phase having the $F\bar{4}3m$ structure: The minor phase is consistent with nanocrystalline Co_3O_4. The values for the ionic radii of Ni^{2+} and Co^{2+} (high spin) are 0.69 and 0.745 Å for six fold coordination, respectively.[23,24] Thus, Co2+ can readily substitute for Ni^{2+} ions in the rock salt structure of NiO. The higher intensity of the (200) peak (located at 43.18°) compared to the usual ratio of peak intensities for bulk NiO suggests somewhat oriented nanocrystalline structures. Rietveld refinement of the XRD data measured from the CSN sample was made in order to further analyze their structural properties. Two $Fm\bar{3}m$ structure CIF files were used in the refinement, one for the NiO core and another for the $Ni_xCo_{1-x}O$ shell, and a $F\bar{4}3m$ structure CIF file for the impurity phase. The lattice parameters and the unit cell volume were found to be increased slightly for the $Ni_xCo_{1-x}O$ shell due to Co doping in the shell region, which is consistent with the ionic radii difference between Ni^{2+} and Co^{2+}. Therefore, Co-incorporation results in a modification of the structure of the shell region of the CSNs, which can indirectly affect the magnetic properties of the $Ni_xCo_{1-x}O$ shell.

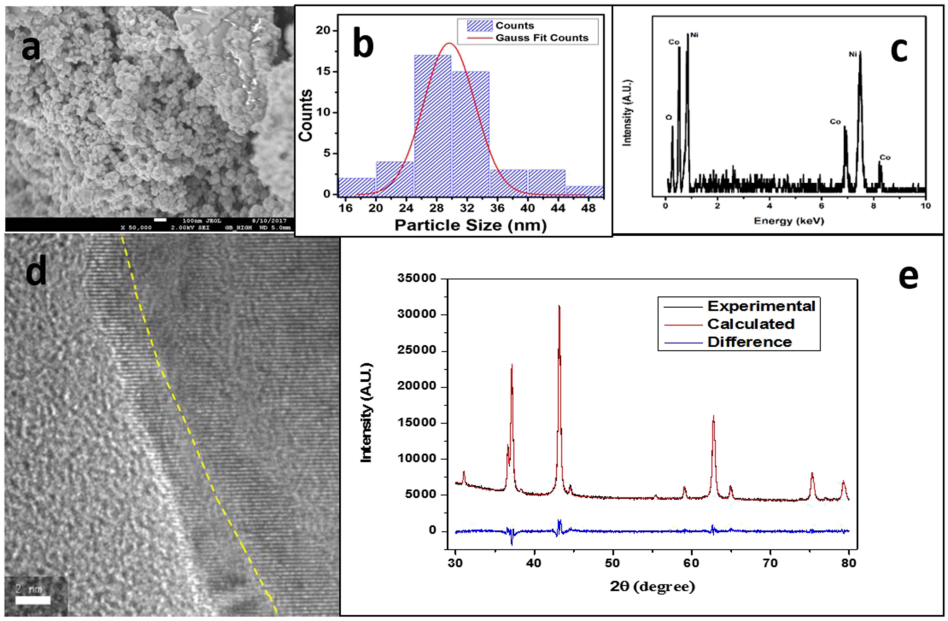

FIG. 1. (a) An SEM image of the core-shell nanoparticles with scale of 100 nm; (b) particle size distribution histogram plot; (c) EDS analysis, (d) a TEM image of CSNs (e) Rietveld refinement profile of the powder XRD pattern of CSNs.

The unusual magnetic behavior may be due to grain size reduction and breaking of large number of exchange bonds. The presence of small magnetic clusters on the surface and lattice imperfection increases the uncompensated spin values.[18]

The magnetization (M) as a function of applied field (hysteresis loop) measured at 5 K is shown in Fig. 2(a). Our preliminary measurements clearly show that the magnetization of the CSNs shows a high retentivity value and does not reach a saturation value at 1000 Oe. The hysteresis shows a coercive field of about ~528 Oe for the ZFC and ~538 Oe for the FC case at 5 K. Ferromagnetism has been reported previously in Co doped NiO nanoparticles by Ponnusamy et al.[18] The hysteresis loops show a shift of the FC hysteresis loop relative to the ZFC loop along the negative H axis and positive M axis directions. This is consistent with an exchange bias between the core and shell regions of the CSNs.[3] The value of the exchange bias is ~34 Oe between FC and ZFC curves based on the formula $H_e = (H_{ZFC+} - H_{FC+} - H_{FC-} + H_{ZFC-})/2$ where the +/- indicate positive/negative H values when M = 0.[25] It is clear that introduction of Co^{2+} ions for Ni^{2+} ions in the NiO structure results in most likely FiM properties within the shell region of the CSNs. The magnetic data for our NiO and Co_3O_4 NPs indicates that these exhibit AFM properties (Fig. 2(c) and (d)). Fig. 2(b) shows the ZFC and FC magnetization vs temperature data measured from our $NiO@Ni_xCo_{1-x}O$ CSNs. The FC magnetization shows a peak at ~20 K followed by a rapid decrease with increasing temperature to ~174 K and a very shallow reduction trend thereafter to 300 K. The ZFC magnetization curve increases sharply from 5 K, peaks at ~20 K and then declines in a similar manner to 300 K as the FC curve but shows a shoulder near ~90 K. The peak at ~20 K is potentially a manifestation of a spin order/disorder transition in the CSNs. The shoulder occurring at ~90 K may be associated with the superparamagnetic blocking temperature of the CSNs. The bifurcation point between the ZFC and FC magnetization curves is at ~100 K.

The supplementary material shows the calculated density of states (DOS) and the partial DOS (pDOS) of the Ni 3d and O 2p orbitals of the NiO and the Ni (Co) 3d and O 2p orbitals of the $Ni_{0.88}Co_{0.12}O$ structures, respectively. The calculated energy band gap is 3.6 eV (defined by the separation between O 2p and Ni t_{2g} orbitals) with the Fermi level positioned at the top of the valence band (VB). Our theoretically calculated band gap value agrees within reason to the experimental value of 3.2–4.0 eV, verifying the validity of our modeling approach. The magnetic moment of Ni was calculated to be 1.7 μB, which is in excellent agreement with experimental results. The Fermi level crosses the majority spin energy states in the upper portion of the VB of the DOS of $Ni_{0.88}Co_{0.12}O$:

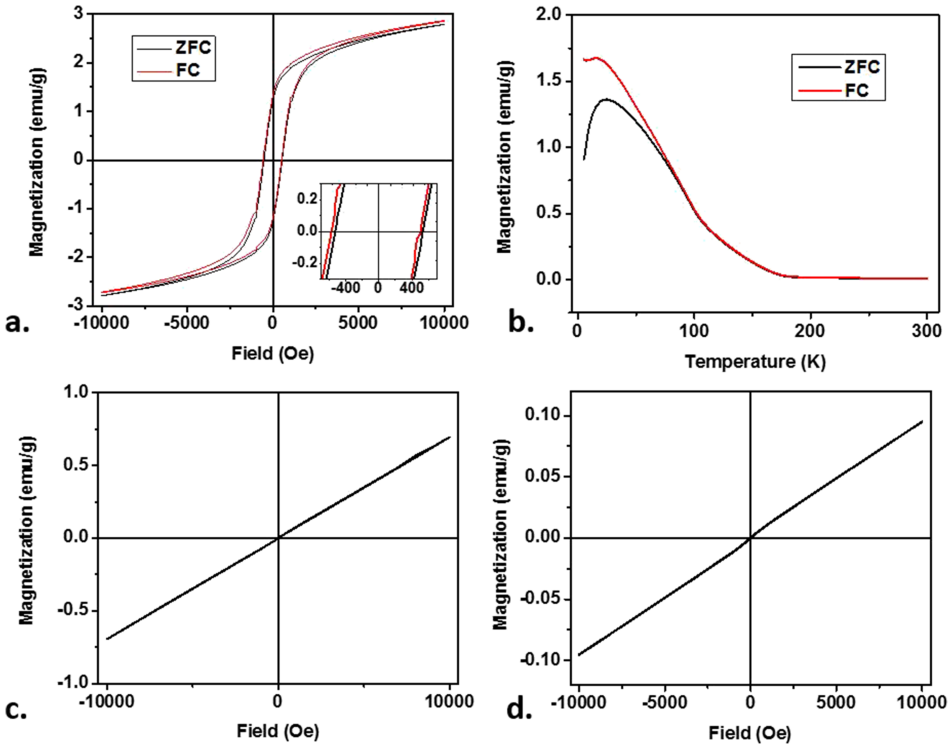

FIG. 2. (a) Zero field cooled (ZFC) and field cooled (FC) magnetization vs applied field (M vs H) measurement data for NiO@$Ni_xCo_{1-x}O$ CSNs (at 5 K temperature): The inset shows the data near the H = 0 Oe region and positive and negative saturation. (b) Magnetization vs temperature data (range 5 K to 300 K) (c) ZFC hysteresis of Co_3O_4 NPs, (d) ZFC hysteresis of NiO NPs.

Because the crossover point occurs in the region where majority Co 3d p-DOS is dominant near the top of VB and majority Ni 3d states occupy the bottom of the conduction band, we conclude that $Co_{0.12}Ni_{0.88}O$ is a Mott-Hubbard insulator (see supplementary material). The introduction of Co in the NiO structure results in the formation of impurity energy levels (IELs), which are dominated by Co 3d states, midway in the band gap. In addition, our calculations show an appreciable shortening of band gap (~2 eV) in $Ni_{0.88}Co_{0.12}O$. It should be noted that the incorporation of Co at such a high percentage (12.5%) is above typical doping levels: Thus, there is a considerable effect in the proportion of Co electronic-level contributions in the DOS of $Ni_{0.88}Co_{0.12}O$, as is evident in the calculated pDOS shown in the supplementary material. The table in the supplementary material shows the calculated individual atomic magnetic moments of the cations in the NiO and $Ni_{0.88}Co_{0.12}O$ structures. Our calculations show that the alternate antiparallel spin arrangement, characteristic of AFM structure, is preserved in the equilibrium spin configuration of $Ni_{0.88}Co_{0.12}O$. However, because of the redistribution of the magnetic moments among the Ni's, and the difference in the Co vs Ni moments, the resultant configuration is weak FiM in the ordered spin state. The incorporation of Co results in a magnetic moment of 0.17 μB/cell in $Ni_{0.88}Co_{0.12}O$. The weak FiM result for $Ni_{0.88}Co_{0.12}O$ from our calculations is consistent with our magnetic measurements made of our CSNs.

IV. CONCLUSIONS

We have used a two-step process, involving thermal decomposition and hydrothermal synthesis, to fabricate NiO@$Ni_xCo_{1-x}O$ CSNs. Our characterization confirms Co incorporation in the shell region of the CSNs. XRD and TEM analysis shows that both core and shell regions have the FCC structure. In addition, the TEM analysis confirms the core-shell structure and epitaxial growth of the shell region over the core region of the NiO@$Ni_xCo_{1-x}O$ CSNs. The magnetometry results are consistent with the presence of an AFM core and an FiM shell in the CSNs exhibiting an exchange bias

effect between the two components as observed by a shift along the applied field and magnetization axes. Our DFT based ab-initio calculations confirm that Co introduction in NiO and formation of $Ni_xCo_{1-x}O$ results in weak FiM properties and in the formation of a Mott-Hubbard insulator.

SUPPLEMENTARY MATERIAL

See supplementary material for DOS-pDOS plots and a table of calculated atomic magnetic moments.

ACKNOWLEDGMENTS

This work was supported in part by the Missouri State University Graduate College. S.H. and R.A.M. acknowledge partial support from the MSU Atwood Award. The Extreme Science and Engineering Discovery Environment (XSEDE) was used for this work, which is supported by the National Science Foundation grant number ACI-1053575.

[1] J. Wang and X. C. Zeng, in Nanoscale Magn. Mater. Appl., edited by J. P. Liu, E. Fullerton, O. Gutfleisch, and D. J. Sellmyer (Springer US, 2009), pp. 35–65.
[2] A. Silva, R. Silva-Freitas, J. Carvalho, T. Pontes, R. Arajo-Neto, K. Silva, A. Carrio, and E. Egito, in Adv. Appl. Biotechnol., edited by M. Petre (InTech, 2012).
[3] A. López-Ortega, M. Estrader, G. Salazar-Alvarez, A. G. Roca, and J. Nogués, Phys. Rep. **553**, 1 (2015).
[4] M. C. Goncalves and M. B. Martins, in *Nanomed* (One Central Press, Manchester, UK, 2014), pp. 83–110.
[5] W. H. Meiklejohn and C. P. Bean, Phys. Rev. **102**, 1413 (1956).
[6] W. H. Meiklejohn and C. P. Bean, Phys. Rev. **105**, 904 (1957).
[7] M. D. Hossain, R. A. Mayanovic, R. Sakidja, and M. Benamara, J. Mater. Res. **32**, 269 (2017).
[8] S. Dey, M. D. Hossain, R. A. Mayanovic, R. Wirth, and R. Gordon, J. Mater. Sci. **52**, 2066 (2017).
[9] M. D. Hossain, S. Dey, R. A. Mayanovic, and M. Benamara, MRS Adv. First View **1** (2016).
[10] L. Del Bianco, F. Boscherini, A. L. Fiorini, M. Tamisari, F. Spizzo, M. V. Antisari, and E. Piscopiello, Phys. Rev. B **77**, 094408 (2008).
[11] H.-C. Hsu, C.-C. Lo, and Y.-C. Tseng, J. Appl. Phys. **111**, 063919 (2012).
[12] A. C. Johnston-Peck, J. Wang, and J. B. Tracy, ACS Nano **3**, 1077 (2009).
[13] M. Patange, S. Biswas, A. K. Yadav, S. N. Jha, and D. Bhattacharyya, Phys. Chem. Chem. Phys. **17**, 32398 (2015).
[14] N. Rinaldi-Montes, P. Gorria, D. Martínez-Blanco, Z. Amghouz, A. B. Fuertes, L. F. Barquín, I. de Pedro, L. Olivi, and J. A. Blanco, J. Mater. Chem. C **3**, 5674 (2015).
[15] C. L. Yuan, J. Phys. Chem. C **114**, 2124 (2010).
[16] E. Skoropata, R. D. Desautels, C.-C. Chi, H. Ouyang, J. W. Freeland, and J. van Lierop, Phys. Rev. B **89**, 024410 (2014).
[17] N. Bayal and P. Jeevanandam, J. Nanoparticle Res. **15**, 2066 (2013).
[18] P. M. Ponnusamy, S. Agilan, N. Muthukumarasamy, M. Raja, and D. Velauthapillai, J. Mater. Sci. Mater. Electron. **27**, 399 (2016).
[19] M. El-Kemary, N. Nagy, and I. El-Mehasseb, Mater. Sci. Semicond. Process. (2013).
[20] S. Hasan, R. A. Mayanovic, and M. Benamara, MRS Advances First View **1** (2017).
[21] A. I. Liechtenstein, V. I. Anisimov, and J. Zaanen, Phys. Rev. B: Condens. Matter Mater. Phys. **52**(8), R5467 (1995).
[22] H. J. Monkhorst and J. D. Pack, Phys. Rev. B: Condens. Matter Mater. Phys. **13**(12), 5188 (1976).
[23] J. P. Perdew, K. Burke, and M. Ernzerhof, Phys. Rev. Lett. **77**, 3865 (1996).
[24] R. D. Shannon, Acta Crystallogr. Sect. A **32**, 751 (1976).
[25] H. Khurshid, S. Chandra, W. Li, M. H. Phan, G. C. Hadjipanayis, P. Mukherjee, and H. Srikanth, J. Appl. Phys. **113**, 17B508 (2013).